Promising regimes for the observation of topological degeneracy in spin chains

Alexander Sattler[*] and Maria Daghofer[†]
Institut für Funktionelle Materie und Quantentechnologien, Universität Stuttgart, 70550 Stuttgart, Germany

(Received 15 February 2024; revised 17 June 2024; accepted 24 June 2024; published 2 July 2024)

Both the Haldane spin chain and a topologically dimerized chain feature topologically protected edge states that are expected to be robust against some kind of noise. To elucidate whether it might be feasible to create such edge states in dimerized chains in a controlled manner in solid states environments, e.g., as spin chains on surfaces, as has already been successfully achieved with the Haldane chain, we investigate their robustness with respect to long-range coupling, anisotropies, and finite chain length. The theoretical investigation is based on an alternating Heisenberg spin chain with spin-1/2, which is investigated using exact diagonalization. We find that dimerized chains and Haldane chains have robustness against long-range coupling and anisotropies. In particular, dimerized spin chains are significantly more robust than Haldane chains.

DOI: 10.1103/PhysRevB.110.024404

I. INTRODUCTION

Topological order and symmetry-protected topological order and their signatures are currently a topic of considerable research interest [1–5], both in noninteracting and in interacting systems, and in one as well as in higher dimensions. A state with topological order can only go over into a topologically trivial one by closing a gap, and surface, edge, or end states are thus an important feature of topologically nontrivial states. Considerable effort is thus spent on realizing and investigating such states, whether in topological states emerging in solids or engineered from other building blocks.

In addition to providing signatures of topological order, surface, edge, and end states are also sought out as a potential use of topological systems. For instance, chiral edges are protected against backscattering [4,5], and helical edge states transport only one spin in each direction [4,5], with uses in spintronics [6–9]. Topological protection has been proposed as a transport channel for quantum information [10,11], and excitations of fractional quantum Hall states can be used in quantum computation [12]. End states of topological spin chains form effective spin-1/2 degrees of freedom and have been conjectured to provide some protection from decoherence [13] and have been proposed as a building block for quantum computation [14].

The Haldane phase [1,2,15–17], a symmetry-protected topological phase based on a conjecture of Haldane [18,19], is an early one-dimensional example for an interaction-based topological scenario. In this chain with spin one, superexchange induces an antiferromagnetic (AFM) coupling between the spins. The resulting AFM ground state is separated from the lowest excitations by a gap, which can be measured by neutron scattering, susceptibility measurements, and magnetization measurement [20–31].

Conceptually, the properties of the Haldane chain can be understood by splitting each spin-1 into two spin-1/2 and then coupling those into singlets [2,15–17,32–40]; see Figs. 1(a) and 1(b). One consequence of this singlet decomposition are the leftover spin-1/2 at the edges, also seen in Fig. 1(b). These are the topologically protected edge states, which leave measurable signature in, e.g., electron spin resonance [30,37,41–43], nuclear magnetic resonance [44], and inelastic neutron scattering [31].

Edge states of Haldane chains were theoretically concluded to also be accessible to scanning tunneling microscopy (STM) [45] and have been successfully measured for both spin-1 chains [46,47] and recently alternating spin-1/2 chains [48,49]. There are several reasons why the ideal scenario can only be approximated: The two edges of finite chains, which can be realized and observed in STM, are coupled, with the coupling between them suppressed exponentially for longer chains. Moreover, magnetic superexchange between spins is not strictly restricted to nearest neighbors and longer-ranged interactions in general increase coupling between the edge states. While they can, in some cases, even be used to decouple edge states from each other on finite chains, this requires delicate fine tuning [50,51]. Finally, signatures of the edge states are rather sensitive to the z-axis anisotropy [45].

A second well-known one-dimensional topological state is the Su-Schrieffer-Heeger (SSH) model [52], where bonds alternate between stronger and weaker coupling. It was originally considered for noninteracting fermions at half filling, where the band structure likewise has zero-energy edge states if the bonds at the ends are weak ones. These can be empty or occupied, i.e., act like a spin-1/2 degree of freedom. For noninteracting bosons or finite onsite interactions, these zero-energy states likewise exist, but next-nearest-neighbor (NNN) hopping moves them away from zero energy [53]. If onsite interactions are infinite, i.e., for hard-core bosons that are in one dimension largely equivalent to fermions [54], the impact of NNN hoppings onto the coupling of the edge states [55] is largely removed. This has recently enabled the observation of the corresponding edge states in a dimerized Rydberg-atom chain [55].

[*]Contact author: alexander.sattler@fmq.uni-stuttgart.de
[†]Contact author: maria.daghofer@fmq.uni-stuttgart.de

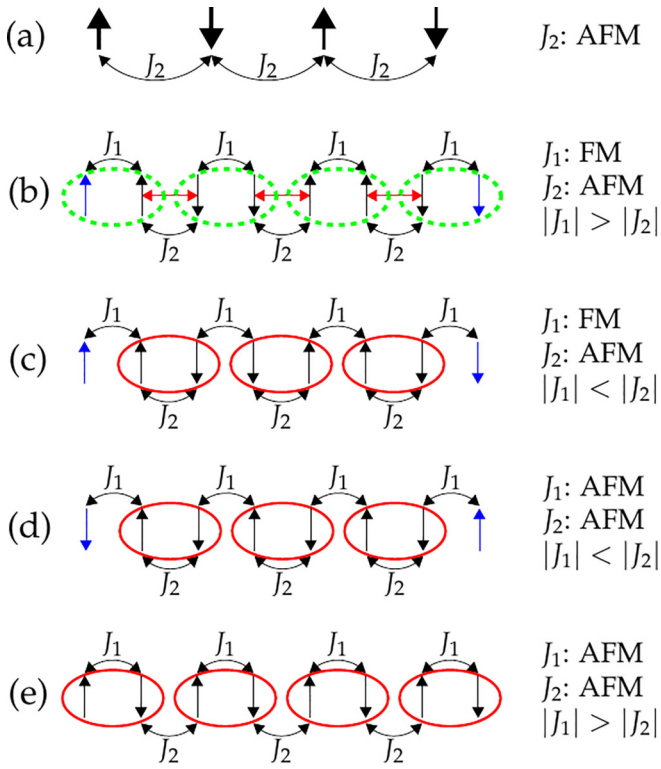

FIG. 1. Sketches for the ground states of a chain of spin-1/2 with alternating Heisenberg exchange couplings J_1 and J_2. In the sketch for the Haldane phase (b), the dashed green ellipses are the effective spin-1, the red arrows indicate their AFM coupling resulting in singlets, and the blue arrows are the free edge spin-1/2. The sketch (a) shows the effective AFM spin-1 chain. The spin-1 in the sketch (a) are the green ellipses in the sketch (b). In the sketches for the dimer phases (c), (d), and (e), the red ellipses are singlets, and the blue arrows are the free-edge spins with spin-1/2.

Here, we investigate edge states of dimerized [33–36,38,39,56–74] spin chains as sketched in Fig. 1. For a strong FM coupling within dimers, the situation becomes clearly similar to Haldane's spin-1 chain; see Figs. 1(a) and 1(b). Indeed, edge modes whose coupling vanishes exponentially with system size have accordingly been investigated [75], and the impact of NNN couplings on the topological phase diagram has likewise been addressed [38,56,60,63,64,67,70]. Strong AFM coupling within as well as between dimers leads to a scenario more similar to the SSH chain [59], sketched in Figs. 1(d) and 1(e). The main theoretical difference to the hard-core bosonic chain is that the latter is equivalent to X-Y spins, while the spin model can include coupling of Z components. [76] As a consequence, positive and negative couplings can no longer be mapped onto each other in the spin model.

Two perfect spin-1/2 edge states imply a fourfold degenerate ground state, as each spin can be flipped without penalty. To be observable, these four states need to be separated from the rest of the spectrum by a gap. While perfect degeneracy cannot be expected for finite chains [77–79], splitting within the lowest four states should be much smaller than the gap separating them from the rest of the spectrum. Since we are here motivated by spin chains in a scanning electron microscope, AFM superexchange couplings are easier to achieve than FM ones. Moreover, the direction perpendicular to the surface is clearly special, so that some z-axis anisotropy is to be expected [13,80–87]. In addition to idealized dimerized chains, we thus also include anisotropies as well as NNN couplings and investigate how they affect ground-state quasidegeneracy.

The paper is structured as follows: In Sec. II we discuss the Hamiltonian of our model. In addition, we introduce our method to distinguish between the topological and the topologically trivial phases. In Sec. III we discuss the results obtained by varying the different parameters in the Hamiltonian introduced in Sec. II. First, we discuss in Sec. III A the inelastic tunneling current accessible to STM. Secondly, we evaluate in Sec. III B spin correlation functions to assess localization of edge modes. Third, we elaborate in Sec. III C on how energy gaps can be exploited as a criterion for edge states and in Sec. III D we use this to discuss various parameter regimes of potential chain realizations. These chains are isotropic and interactions are limited to the nearest neighbor. We show how to use the method, see Sec. II, to characterize topological phase transitions by analyzing different energy gaps between the lowest energies. In the subsequent sections, we look at the impact of various perturbations of this ideal scenario. We start with the NNN coupling in Sec. III E, investigate z-axis anisotropy in Sec. III F, and combine both in Sec. III G. Sec IV concludes the paper and gives a summary of the results obtained as well as an outlook to promising future studies.

II. MODEL AND METHODS

We start from an idealized dimerized [33–36,38,39,56–74] chain with nearest-neighbor (NN) couplings

$$H = J_1 \sum_{i=1}^{N/2} \left(S^x_{2i-1}S^x_{2i} + S^y_{2i-1}S^y_{2i} + \Delta_z S^z_{2i-1}S^z_{2i}\right) + J_2 \sum_{i=1}^{N/2-1} \left(S^x_{2i}S^x_{2i+1} + S^y_{2i}S^y_{2i+1} + \Delta_z S^z_{2i}S^z_{2i+1}\right), \quad (1)$$

where J_1 and J_2 are the inter- and intradimer couplings, Δ_z gives their z-axis anisotropy and N is the number of spins. $\Delta_z \gg 1$ leads to more Ising-like spins while $\Delta_z \ll 1$ would imply x-y anisotropy. Topological phases only occur with an AFM [66] $J_2 > 0$, see Fig. 2, and we use J_2 as our unit of energy, i.e., $J_2 = 1$. Since we are interested in edge states, we use open boundary conditions (OBC), so that edge states equivalent to $S = \frac{1}{2}$ [see Figs. 1(b)–1(d)] imply a fourfold degenerate ground state [77–79].

These terms are complemented by NNN coupling [38,56,60,63,64,67,70]

$$H_{\mathrm{NNN}} = J_{\mathrm{NNN}} \sum_{i=1}^{N-2} \left(S^x_i S^x_{i+2} + S^y_i S^y_{i+2} + \Delta_z S^z_i S^z_{i+2}\right). \quad (2)$$

In addition, there can be an uniaxial single-ion anisotropy [13,16,18,34,88–90] (D anisotropy),

$$H_{\mathrm{D}} = D \sum_{i=1}^{N/2} \left(S^z_{2i-1} + S^z_{2i}\right)^2, \quad (3)$$

where D is the strength of the anisotropy.

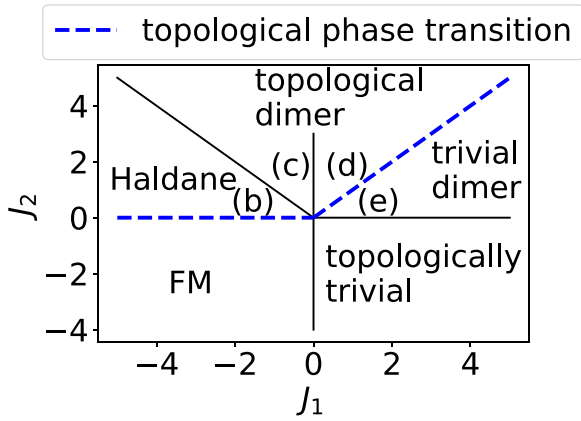

FIG. 2. Phase diagram for an even number of spins of an infinite alternating Heisenberg spin chain with the alternating coupling constants J_1 and J_2. The dashed blue lines show the topological phase transition. Labels (b)-(e) refer to the sketches shown in Fig. 1, which schematically illustrate the ground states.

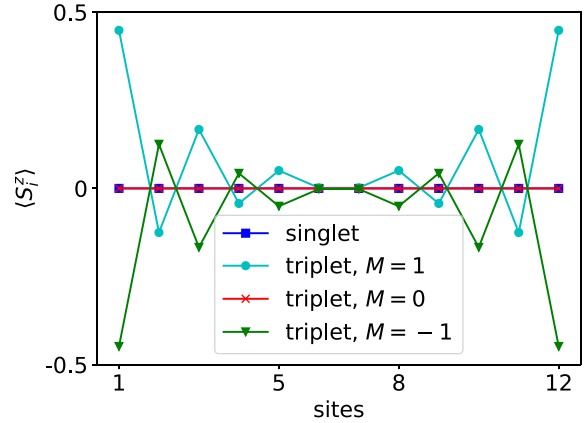

FIG. 3. Expectation value $\langle S_i^z \rangle$ of the singlet and triplet states of the edge modes for an isotropic chain consisting of 12 spins, with $J_1 = 0.5$ and without NNN couplings. The properties of the four ground states are well recognizable.

A standard method to distinguish between the topologically trivial and nontrivial phases is the string order parameter [34,36,38,39,56,59,66,73,91] introduced by Nijs and Rommelse [92] and Tasaki [93]. However, it is only cleanly defined for infinite chains, while we are here explicitly interested in finite ones. Moreover, our focus is mostly on the edge states in imperfect systems, where they arise, and how robust they are. Consequently, we use the (approximate) fourfold degeneracy of the ground state, which is an important property of the topological state of a chain with OBC, as a criterion.

We investigate the Hamiltonian by using exact diagonalization (ED) of chains, whose length is comparable to the number of spins that can be assembled in an STM [46,80,81,83,87,94,95]. Chains of, e.g., 12 spins are accessible to full numerical diagonalization. In some cases, we go to longer chains to assess finite-size effects, which can be strong for short chains [77–79,96], and then use a band-Lanczos algorithm [97]. In this variant of the standard Lanczos approach, several starting vectors are used at the same time and are mutually orthogonalized. While the plain Lanczos algorithm cannot reliably resolve (near) degeneracies [97], we can thus determine them as long as the number of starting vectors is greater than the degeneracy.

III. RESULTS

Figure 3 shows the expectation value $\langle S_i^z \rangle$ of the singlet and triplet states of the edge modes, see Fig. 1(d), where S_i^z is the spin operator of the ith spin in the chain. The triplet states with $M = \pm 1$ have, exactly as expected, $\langle S_i^z \rangle \approx \pm 1/2$ at the edges and $\langle S_i^z \rangle$ decays exponentially towards the bulk of the chains, following a pattern analogous to that observed in the $S = 1$ AFM chain [98]. The stronger the dimerization (i.e., the smaller $|J_1|/J_2$), the smaller the difference $||\langle S_i^z \rangle| - 1/2|$ at the edges. The impact of N on $\langle S_i^z \rangle$ is small compared to the effect of dimerization strength.

Energy splitting as a criterion can be motivated by the goal of observing an edge state. For instance, consider the time evolution of a low-energy state prepared to have spin "up" at the left edge, which can be obtained by combining three of the four quasidegenerate low-energy states, see Fig. 3, as

$$|i\rangle = \frac{1}{\sqrt{2}}\Big(|S = 1, M = 1\rangle + \frac{1}{\sqrt{2}}(|S = 1, M = 0\rangle + |S = 0, M = 0\rangle)\Big). \quad (4)$$

As can be seen in Fig. 4 at time $t = 0$, the z component of the spin on the right edge then averages to zero. Experimentally, one might expect such a state if the temperature is low enough to bring the chain into its quasidegenerate low-energy manifold, but if a magnetic tip polarizes one edge. Time evolution can then be calculated using ED.

Figure 4 shows the time evolution of $\langle S_i^z \rangle$ and compares a Haldane-like scenario (i.e., with a strong FM J_1) to a dimer-scenario. One sees that in both cases, the positive spin remains on the left edge for relatively long times before tunneling to the right edge. The tunneling time is inversely proportional to the energy difference between the singlet and triplet states,

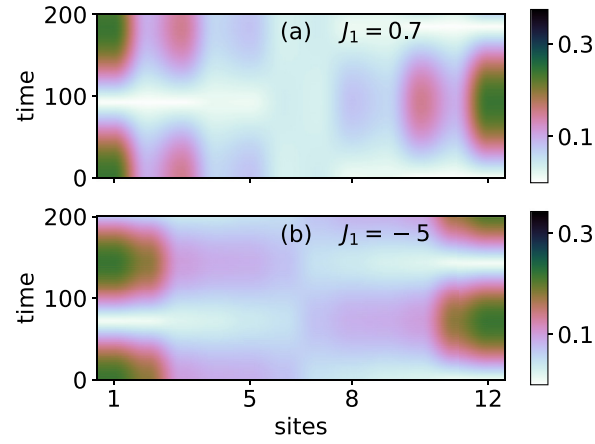

FIG. 4. Expectation value $|\langle S_i^z \rangle|$ of the time evolution of a state Eq. (4) prepared to have $\langle S_i^z \rangle = \frac{1}{2}$ on the left edge for (a) the dimer scenario with $J_1 = 0.7$ and (b) the Haldane scenario with $J_1 = -5$.

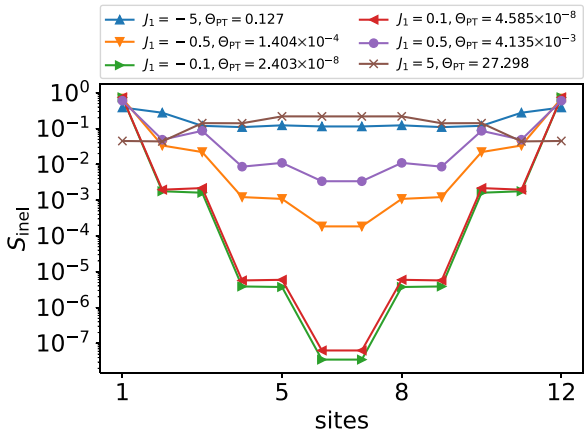

FIG. 5. Inelastic signal Eq. (5) for isotropic chains with 12 spins and without NNN couplings. For comparison between both phase transition criteria, there are in the legend the values of Θ_{PT}; see Eq. (7).

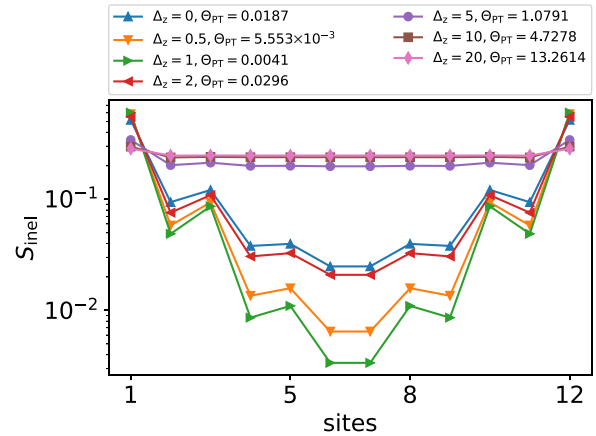

FIG. 6. Inelastic signal Eq. (5) for an anisotropic chain with 12 spins, without NNN couplings and D anisotropy. The coupling constant is $J_1 = 0.5$. For comparison between both phase transition criteria, there are in the legend the values of Θ_{PT}; see Eq. (7).

i.e., directly related to the splitting within the quasidegenerate manifold, respectively, the coupling of the edge modes. As the gap between the singlet and triplet states decreases with increasing N, as shown in Fig. 12, the tunneling time rises.

Due to the finite length of the spin chains, there is an energy gap between the singlet and the triplet states; see Fig. 10. The singlet state is the ground state if J_1 and J_2 are AFM. A chain with FM J_1 and AFM J_2 has a singlet ground state if $N/2$ is even and a triplet ground state if $N/2$ is odd. This can be explained by the Lieb-Mattis theorem [99,100].

A. Inelastic tunneling current and spin spectral density

Inelastic electron tunneling spectroscopy can be used to measure edge states with an STM [46]. Excitation from the singlet (triplet) ground state into the nearly degenerate triplet (singlet) state is found at an energy close to zero if the edge states are indeed independent of each other. The expected signal is proportional to the matrix elements [45,46,84,86] describing such transitions

$$S_{\text{inel}} = \sum_{\alpha,j} |\langle \text{SG}|S_i^\alpha|\text{TP}_j\rangle|^2, \tag{5}$$

where $|\text{SG}\rangle$ is the singlet state and $|\text{TP}_j\rangle$ with $j = 1, 2, 3$ are the triplet states formed by the edge spins; see Figs. 1(b)–1(d). S_i^α is the spin operator for component $\alpha = x, y, z$ of the ith spin in the chain.

For a spin-1 Haldane chain, the signal is indeed found to be stronger on the first and last spin [45], by the ratio of about four, so that it can be used to detect edge states. Figure 5 shows the matrix-element weight Eq. (5) for a 12-site chain and varying J_1. In the topological regime $J_1 < J_2$, weight is consistently concentrated on the edges, while it is found in the bulk for the trivial $J_1 = 5\, J_2$. One also sees that the localization of the edges becomes more pronounced in the dimer regime with $|J_1| < J_2$ than it is in the Haldane regime with $J_1 < -1$; see Fig. 2. This suggests that dimerized chains might be a good place to investigate edge states.

Figure 6 shows the impact of a z-axis anisotropy on the inelastic signal Eq. (5) for a dimerized chain. The signal continues to be located at the edges also for strong anisotropies Δ_z [see Eq. (1)]. It is possible to drive the excitation from the edge into the bulk, but very strong anisotropies (e.g., $\Delta_z = 10$) are needed to achieve a signal (almost) uniformly distributed over the chain.

The most significant difference in the inelastic signal occurs between the edge spins and the spin farthest from the edges. As this distance grows with N, the disparity in the inelastic signal between the center of the chain and its edges increases by several orders of magnitude. Nonetheless, the edge signal is more pronounced for dimerized chains than for the Haldane regime at any N.

However, even when transitions between the four lowest states are localized at the edges, the site-dependent inelastic signal Eq. (5) can only be useful if any bulk excitations are at appreciably higher energies. This translates into the requirement that the four low-energy states are separated from the rest of the spectrum by a gap. Information on edge states and energy gaps is combined in Green's functions, i.e., in dynamic spectra of the form

$$S_i(\omega) = \sum_{m,\alpha} |\langle m|S_i^\alpha|0\rangle|^2 \delta(\omega - (E_m - E_0)). \tag{6}$$

Operator S_i^α denotes as above spin component $\alpha = x, y, z$ at site i and $|0\rangle$ is the ground state with energy E_0. In contrast to Eq. (5) above, the sum runs over all excited states $|m\rangle$ with energy E_m, not just the quasidegenerate triplet. We use the Lanczos algorithm to numerically obtain spectra [101,102].

Spectra shown in Fig. 7 for a Haldane-like chain again show the low-energy excitations located almost exclusively at the end sites, with only a little weight leaking into the chain. Higher-energy excitations into states beyond the quasidegenerate ground-state manifold are also seen within the chain, their energy corresponds to the gap between the fourth and fifth eigenstates of the chain (see Fig. 10). As found previously [45], even rather small z-axis anisotropy of $\approx$1 % is enough to allow a substantial part of the edge-state weight to leak into the bulk; see Figs. 7(b) and 7(c).

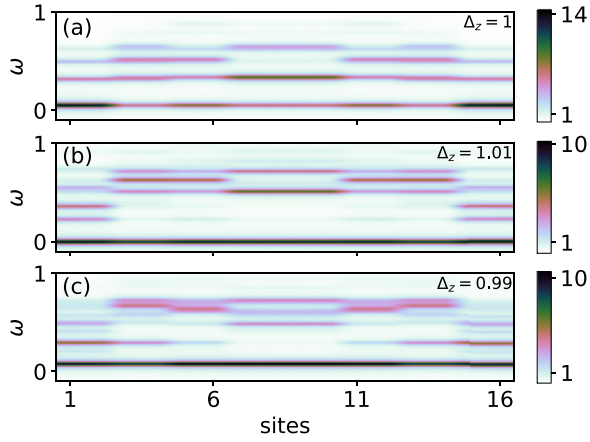

FIG. 7. Site-dependent spin-excitation spectra Eq. (6) for $J_1 = -5$ (Haldane scenario). Panel (a) is the isotropic chain, i.e., $\Delta_z = 1$, (b) $\Delta_z = 1.01$, and (c) $\Delta_z = 0.99$. $J_{\mathrm{NNN}} = 0$ and $D = 0$ in all cases.

The higher-energy states that come down in energy at the same time are, however, also found rather close to the edges. This implies that the identification of edge states using the inelastic signal can only be a first step: The site-dependent low-energy weight can still be enhanced near the edges, even though the object at the edge consists of several excitations and is no longer similar to a spin 1/2.

Figures 7(b), 7(c) and 8(b), 8(c) compare the impact of z anisotropy Δ_z [see Eq. (1)] on the dimer and Haldane scenarios. The low-energy edge states move into the chain already for small deviations from $\Delta_z = 1$ in the Haldane scenario; see Figs. 7(b) and 7(c). In contrast, they remain clearly localized in the dimer cases Figs. 8(b) and 8(c), just as in the case of the isotropic dimer scenario Fig. 8(a).

The more pronounced and robust spin-excitation spectrum at the edges for dimerized chains, in comparison to Haldane-like chains, is independent of N. However, there are finite-size effects: Larger N increases spin-excitation spectra at the edges

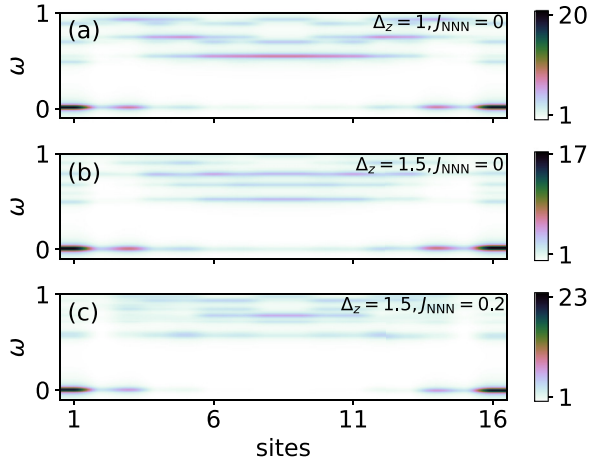

FIG. 8. Site-dependent spin-excitation spectra Eq. (6) for $J_1 = 0.7$ (dimer scenario). The remaining parameters are (a) $J_{\mathrm{NNN}} = 0.0$, $\Delta_z = 1$, (b) $J_{\mathrm{NNN}} = 0.0$, $\Delta_z = 1.5$, and (c) $\Delta_z = 1.5$, $J_{\mathrm{NNN}} = 0.2$. $D = 0$ in all cases.

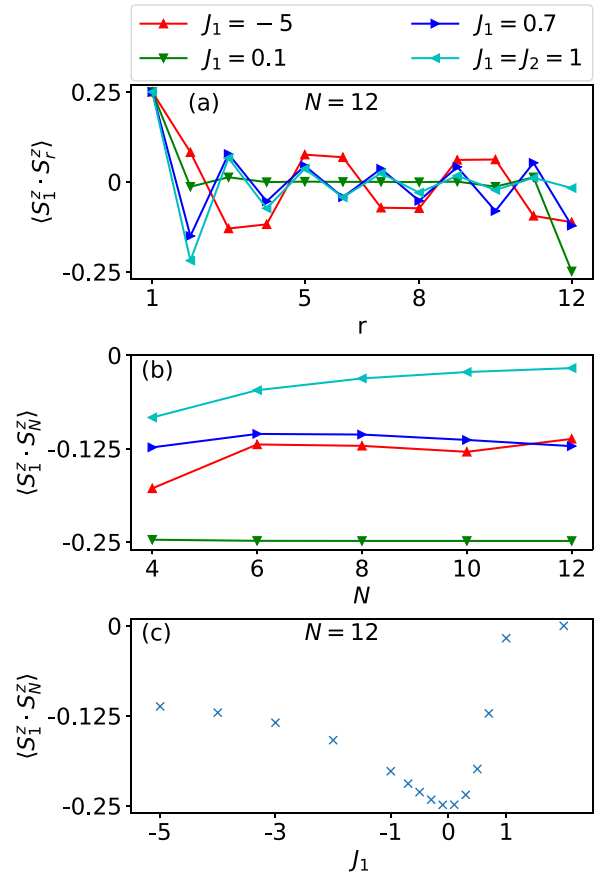

FIG. 9. Static spin-spin correlation functions for the (singlet) ground state. Panel (a) gives correlations depending on distance for $N = 12$. Panels (b) and (c) give the edge-edge correlations depending on N and J_1, respectively.

while it decreases them in the bulk. Additionally, spectra at higher energies decrease with increasing N.

B. Correlation functions

To some extent, edge-state localization can also be inferred from static correlation functions. Figure 9(a) shows the correlation between one edge spin and the other sites of an $N = 12$-site chain. For the uniform chain with $J_1 = 1$, their absolute value decreases with growing distance, so that the two edge spins are the spins least correlated to each other. For $J_1 = 0.1$, in contrast, correlations fall off extremely fast, remain essentially 0 throughout most of the chain, and recover nearly the most correlated value possible, namely -0.25, for the other edge.

In addition to these extreme cases with and without localized edge states, correlations are shown for $J_1 = 0.7$ (dimer phase close to the topological phase transition) and $J_1 = -5$ (Haldane regime). For $J_1 = 0.7$, correlations fall of slowly with distance and first resemble those for $J_1 = 1$. However, they *grow* again in the second half of the chain instead of falling off further. This illustrates that some edge-state physics can still be observed. The Haldane chain shows similar growth in the second half, i.e., edge-state correlations are present, albeit weak. Figure 9(b) shows the edge-edge correlations

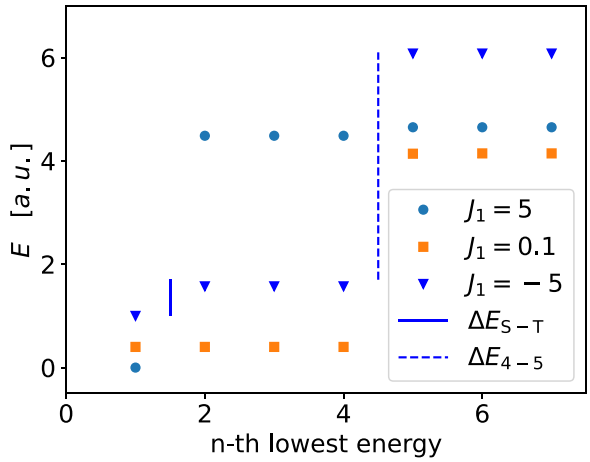

FIG. 10. Lowest few energies depending on J_1 for an isotropic spin chain with 12 spins and $J_{NNN} = 0$. There are two important energy gaps. First, ΔE_{S-T}, the energy gap between the singlet and the triplet states, and second ΔE_{4-5}, the energy gap between the fourth and the fifth lowest energy. The gap ΔE_{S-T} is tiny in the case of a strong dimer formation $J_1 = 0.1$. For a weak dimer formation and in the Haldane phase, e.g., $J_1 = -5$, this energy gap is increasing, but there remains a quasi fourfold degenerate ground state. In the topologically trivial phase, e.g., $J_1 = 5$, there is a nondegenerate ground state.

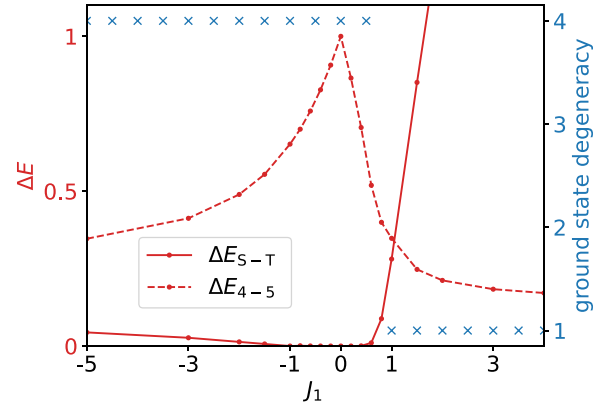

FIG. 11. Lowest few energies depending on J_1 for an isotropic spin chain with 12 spins and $J_{NNN} = 0$. There are shown the energy gaps ΔE_{S-T} and ΔE_{4-5}, as introduced in Fig. 10. The gap ΔE_{S-T} is tiny in the case of a strong dimer formation $|J_1| \ll 1$. For a weak dimer formation and in the Haldane phase this energy gap is increasing, but there remains a quasi fourfold degenerate ground state. In the topologically trivial phase, i.e., $J_1 \geqslant 1$, there is a nondegenerate ground state. The fourfold degeneracy resolves at the topological phase transition at $J_1 = 1$.

depending on N for the four cases, with only small finite-size effects.

Finally, Fig. 9(c) depicts the edge-edge spin correlations depending on J_1. As suggested by Fig. 9(a), they become very strong in the dimer regime $|J_1| \to 0$, remain sizable but smaller in the Haldane-like scenario $J_1 \ll 0$, and approach 0 for $J_1 \to 1$. Comparing edge-edge correlations to edge-bulk correlations can thus be used as a criterion for topological edge states even for modest chain sizes.

C. Energy gaps as a criterion for edge states

The information on energy gaps discussed in the figures above can be summarized into a parameter given by the ratio of gaps in the eigenvalue spectrum of the Hamiltonian. Leftover spins $S = \frac{1}{2}$ at the edges, see Figs. 1(b)–1(d), which are decoupled for infinite chains, will become coupled in realistic short chains, which splits the fourfold degenerate ground state into a singlet and a triplet [46,77–79]. To consider the edge states as still "approximately decoupled," the singlet-triplet gap should be smaller than the gap ΔE_{4-5} separating the fourth from the fifth state; see Fig. 10.

Figure 10 illustrates the concept, see Eq. (7), to distinguish between topological and topologically trivial phases. One sees example spectra for two cases with an approximate ground-state degeneracy ($J_1 = -5$ and $J_1 = 0.1$) and one without edge states ($J_1 = 5$). We evaluate

$$\Theta_{PT} := \begin{cases} \max\limits_{i=1,2,3} \frac{\Delta E_i}{\Delta E_{4-5}} & \text{if } D_{GS} \leqslant 4, \\ \frac{\Delta E_{GS}}{\Delta E_{4-5}} & \text{otherwise,} \end{cases} \tag{7}$$

where D_{GS} is the (quasi)degeneracy of the ground-state manifold and ΔE_{GS} is the energy gap above the ground state. More generally, the singlet-triplet gap will later be replaced by the largest gap within the lowest four states.

We then define transitions where the ratio Θ_{PT} crosses a certain value Θ_{PT}^{tran}. This serves as an indicator where edge states might be expected to be sufficiently protected to be observable. While the exact value of the threshold is certainly open to debate, our primary outcomes do not qualitatively change when Θ_{PT}^{tran} is varied. Here, we use $\Theta_{PT}^{tran} = 0.5$. To illustrate the use of the parameter, Θ_{PT} values [see Eq. (7)] for each chain are given in Figs. 5 and 6. $\Theta_{PT} \ll \Theta_{PT}^{tran}$ consistently holds for spin chains where the inelastic signal is localized at the edges. Spin chains with an inelastic signal concentrated at the edges always have a quasidegenerate ground state, while no such degeneracy exists for spin chains with a large inelastic signal in the bulk.

D. Gaps for the isotropic alternating chain

Figure 11 shows the two crucial energy gaps, as introduced in Fig. 10, depending on J_1. For negative (i.e., FM) value of J_1, the ΔE_{S-T} is always much smaller than ΔE_{4-5}, so that the system remains in the topological (Haldane) phase. However, ΔE_{S-T} grows and ΔE_{4-5} shrinks, reflected in the ratio Eq. (7) and making the system less suitable for observation of the edge states. For positive J_1, in contrast, we find in Fig. 12 a sudden transition from quite small Θ_{PT} to $\Theta_{PT} > 1$ at the topological phase transition, where the quasi fourfold ground-state degeneracy is lost.

Since finite spin chains are analyzed, finite-size effects are a concern. Figure 12 shows the energy gaps discussed in Fig. 10 as well as their ratio Θ_{PT}, depending on the chain length N. While the gap ΔE_{4-5} remains finite for longer chains, ΔE_{S-T} is strongly suppressed within the topological regime once chains become longer than about eight sites. This suggests that the edges can be considered to be approximately decoupled even on rather short chains. The ratio given in the

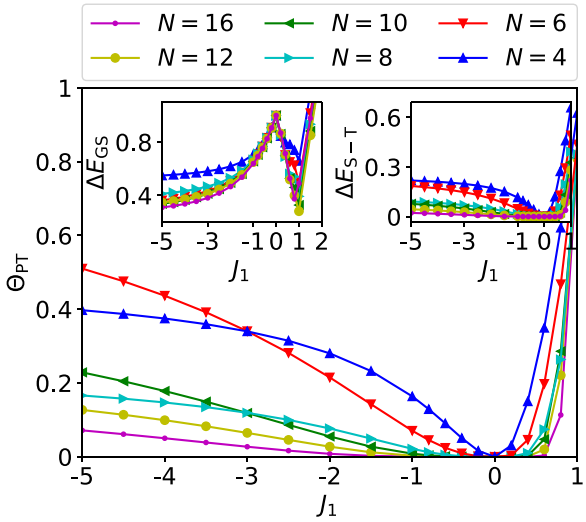

FIG. 12. Edge-state interaction depending on chain length. The results belong to an isotropic spin chain without NNN coupling. The left inset shows the energy gap above the ground state ΔE_{GS}. This gap has a minimum $J_1 = 1$. The right inset shows $\Delta E_{\mathrm{S-T}}$ (see Fig. 10). The ratio, see Eq. (7), between the energy gap inside the quasidegenerate ground state and the energy gap above the ground state is shown in the large figure.

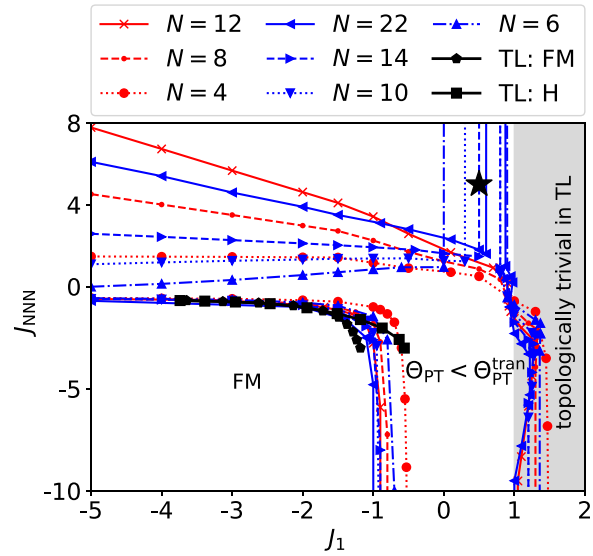

FIG. 13. Impact of NNN coupling depending on chain length. In the topological dimer phase, much stronger FM NNN couplings are possible than in the Haldane phase. The finite-size effects for AFM NNN coupling show a fundamental difference between $N/2$ even and $N/2$ odd. For comparison, phase transition out of the Haldane phase (TL: H) and into the FM phase (TL: FM) were extracted from Refs. [64,67] for the TL. (In the TL there are intermediate phases between the FM and the topological phase. In the regime marked with ★, where $J_{\mathrm{NNN}} \gg J_{1,2}$, chains with $2(2n+1)$ sites have a nearly fourfold degenerate ground state, but do not feature protected edge states. Instead, two nearly decoupled subchains each have half-integer spin and thus a spin-1/2 doublet ground state, combining to four states. Coupling between chains grows with system size, so that this approximate degeneracy is lifted in the TL. There is a topological phase transition in the TL at $J_1 = J_2$, as shown in Fig. 2. Further discussion about finite-size effects can be found in Appendix.

main panel of Fig. 12 gives accordingly a consistent picture except for the very shortest chains.

E. Next-nearest-neighbor coupling

Since the gap ratio Eq. (7) summarizes information on the relevant energy scales conveniently and also works for finite chains, we use it to delineate regimes where one can hope to observe edge states even in imperfect systems. We first look at the impact of NNN coupling, see Eq. (2), as analogous hopping is known to destroy ground-state degeneracy for non-interacting bosons.

For FM NNN coupling, substantial differences between "Haldane" and "dimer" regimes arise; see Fig. 13. In the former, where stronger $|J_1| > |J_2|$ stabilizes the quasi-spin-1 constituents [see Figs. 1(a) and 1(b)], even rather weak $J_{\mathrm{NNN}} < 0$ is enough to drive a topological phase transition to a (trivial) FM state. In the topological dimer phase (i.e., where AFM J_2 is stronger than $|J_1|$), there is no such transition. Thus, the topological dimer phase is significantly more robust than the Haldane phase against FM NNN coupling.

For AFM NNN coupling, finite-size effects are substantial and show pronounced even/odd differences, i.e., between even and odd $N/2$, especially in the Haldane phase. Depending on chain length, either small values of $J_{\mathrm{NNN}} > 0$ couple edge spins, or even quite large ones leave them uncoupled. For long chains and strong FM J_1, AFM $J_{\mathrm{NNN}} > 0$ can, however, be allowed to become quite large without affecting edge-state degeneracy. This fits with earlier observations that NNN coupling can be used to tune edge-state coupling in Haldane chains [50,51].

In addition to the Haldane phase, other topological phases are predicted to arise in alternating FM-AFM chains with FM NNN coupling [64,67]. Figure 13 also includes the thermodynamic-limit (TL) phase transitions from the Haldane phase ("TL: H") to intermediate spin-gap phases and the transition from these phases to the FM phase ("TL: FM"), extracted from Refs. [64,67]. For the chain parameters of these intermediate phases, we mostly still observe an approximately fourfold degenerate ground state. However, finite-size effects are small in this regime $J_{\mathrm{NNN}} < 0$.

F. Spin anisotropy Δ_z of couplings and uniaxial single-ion–like anisotropy D

Next, we will address spin anisotropies that select a specific axis. The first purpose is to investigate the connection to the hard-core bosons of Ref. [55], which correspond to $\Delta_z = 0$ in our spin model. The second reason is that such anisotropies have to be expected for spins on surfaces [13,80–87] and have been shown to strongly affect edge states of Haldane chains [45].

We model two sources of anisotropy: (i) coupling anisotropy Δ_z affecting all spin-spin couplings, see Eq. (1), and (ii) "single-ion" anisotropy D of Eq. (3) affecting only the J_1 bonds. Turning these bonds FM moves our model into the "Haldane-like" phase and $D < 0$ ($D > 0$) then favors

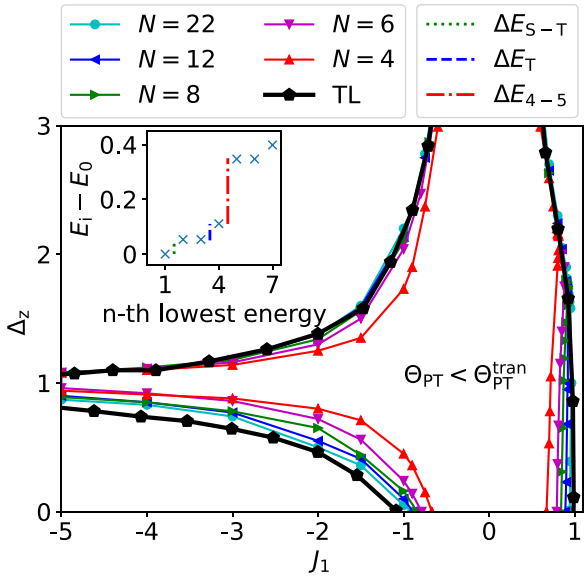

FIG. 14. z anisotropy for chains without NNN coupling or D anisotropy depending on the chain length. The topological dimer phase is more robust than the Haldane phase. The finite-size effects are small. The inset shows the low energy spectrum, which is shifted by the ground-state energy E_0. TL phase boundaries shown in black were extracted from Ref. [103].

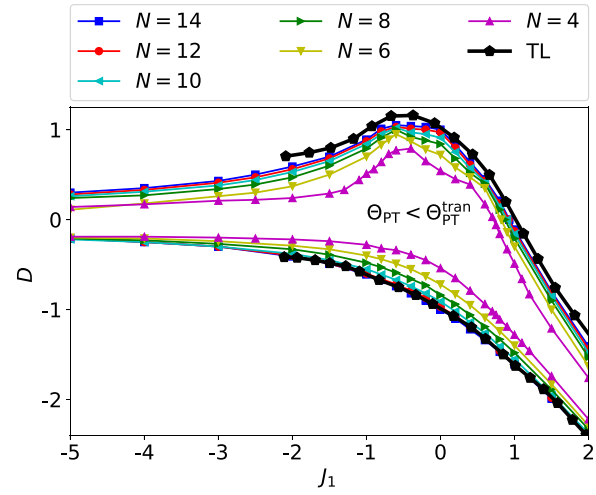

FIG. 15. D anisotropy for chains without NNN coupling or z anisotropy depending on chain length. The topological dimer phase is more robust than the Haldane phase. The finite-size effects are small. TL phase boundaries in black were extracted from Ref. [34].

states with $S_z = \pm 1$ ($S_z = 0$) of a local triplet, as a single-ion anisotropy [45,78] would.

Figure 14 shows the influence of a z anisotropy on chains without NNN coupling or D anisotropy. Due to z anisotropy Δ_z, see the Hamiltonian Eq. (1), the triplet splits in a singlet and a doublet, as shown in the inset of Fig. 14. There is thus an additional energy gap ΔE_T within the quasidegenerate ground-state manifold, in addition to the energy gaps of Fig. 10. The phase diagram in the main panel has only a relatively minor finite-size effects, especially in comparison to the large finite-size effects for NNN coupling, as discussed in Fig. 13. More importantly, edge-state degeneracy can be found for a large part of the phase diagram.

For $\Delta_z = 0$, which corresponds to hard-core bosons, the topological regime with detectable edge-state degeneracy is mostly confined to $|J_1| \lesssim J_2$. For $\Delta_z > 0$ which has to be expected for spin implementations, edge states are first stabilized up to the isotropic regime $\Delta_z = 1$. Beyond this point, i.e., for Ising-like anisotropy, the stability regime of edge-state degeneracy shrinks again but remains sizable; see Fig. 14.

Figure 15 shows the impact of single-ion-like D anisotropy; see Eq. (3). Again, finite-size effects are moderate, although the topological phase increases with chain length. Similar to Δ_z (see Fig. 14), edge-state degeneracy is remarkably robust. Again, this robustness is most pronounced for the dimer regime, while edge states in the Haldane-like regime at $J_1 < -1$ (see Fig. 2) are more easily destroyed.

The most striking and relevant result is that the topological dimer phase is remarkably robust against both types of z anisotropy. Similar to FM NNN coupling, this robustness is enhanced even for FM J_1. Edge-state degeneracy is here much better protected than in the Haldane-like spin-1 regime at large $|J_1| \gg 1$; see Fig. 14. Robustness extends to $\Delta_z < 1$ (x-y symmetry) and $\Delta_z > 1$ (Ising symmetry). The latter is particularly encouraging because spins on surfaces usually have a z anisotropy [13,81–87].

G. z anisotropy and NNN coupling

Finally, we consider the interplay of NNN coupling and z-axis spin anisotropy. As a result of a "single-ion-like" anisotropy affecting only J_1 bonds are similar to Δ_z affecting all bonds, see above in Sec. III F, we focus here on Δ_z anisotropy; see Eq. (1).

The stability regions of quasidegenerate edge states are shown for various values of J_1 and eight-site chains in Fig. 16(a) and with 16 spins in Fig. 16(b). Data inherit here the pronounced finite-size effects observed for NNN coupling in Sec. III E, as well as the even/odd effects with odd or even $N/2$. For visibility, the Δ_z axis is split into small and large regimes in Fig. 16.

For the Haldane regime with $J_1 = -2$, only relatively small Δ_z and FM $J_\mathrm{NNN} < 0$ are allowed, while a larger range of AFM $J_\mathrm{NNN} > 0$ are acceptable, both in agreement with results discussed earlier (see Fig. 13 and Fig. 14). In the dimer regime $J_1 = -0.8$, stability w.r.t. Δ_z increases immediately and markedly. J_NNN must now not become quite as large, but would still need to be unrealistically large $J_\mathrm{NNN} > J_1$ to destroy quasidegeneracy. Moreover, $J_\mathrm{NNN} < 0$ is now also possible, which again illustrates that edge states are far better protected in the dimer regime.

Even for very large values of $\Delta_z \gg 1$, the protected edge states can be found for some (albeit narrow) range of $J_\mathrm{NNN} \approx J_1/2$. However, this only applies to the dimer regime, but not to Haldane-like chains. This may be related to the frustration, caused by competing NN and NNN couplings. When comparing the robustness between chains with and without frustration, it can be seen that frustrated chains tend to have more robust edge-state degeneracy, so that a larger $|\Delta_z - 1|$ is possible.

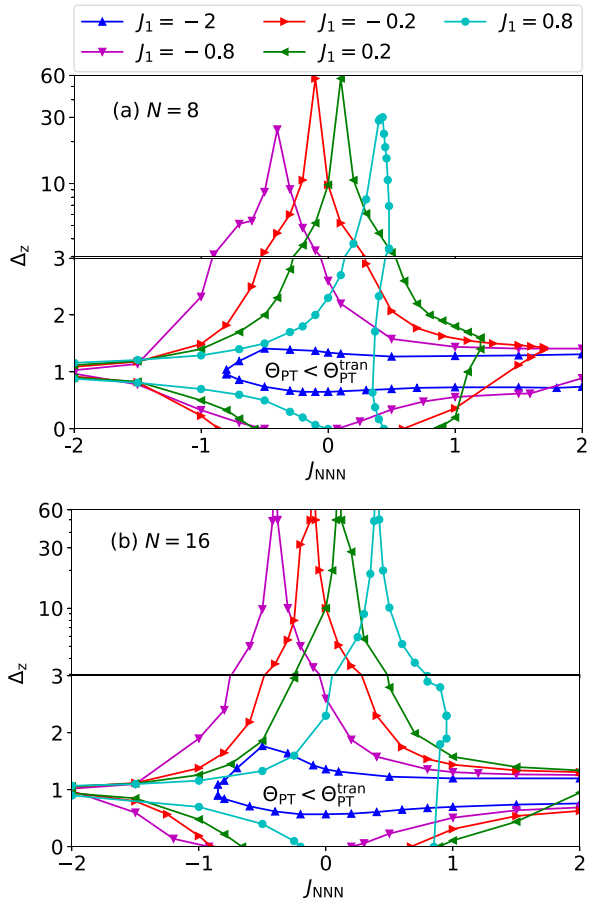

FIG. 16. Combination of z anisotropy with NNN coupling for a chain with (a) 8 and (b) 16 spins.

IV. DISCUSSION AND CONCLUSIONS

We have investigated how well edge states of topologically nontrivial one-dimensional spin chains are protected in finite chains and for deviations from the ideal model Hamiltonians. To do so, we compared the energy gap(s) within the four lowest eigenstates, which is due to coupling of the edge states and vanishes for the ideal case, to the "topological" energy gap separating these four states from the rest of the spectrum.

We focus our investigations explicitly on finite chains, as we aim to identify regimes where topological degeneracy is visible on chains short enough to be assembled in an STM. Perfect fourfold degeneracy is not observed in the ground state, but a quasidegeneracy in finite chains can closely approximate perfect degeneracy, especially deep in the dimer phase. The splitting within the four lowest-energy states is here much smaller than their separation from the rest of the spectrum.

Spin correlation functions can be used to illustrate localization of edge modes. Even in short chains, topological edge modes are clearly localized, as we discuss in Sec. III B. The correlation of spins between edges is notably more pronounced in the topological dimer phase compared to the Haldane-like phase and increases with stronger dimerization. As edge-edge correlations increase, edge-bulk correlations diminish. In contrast, the inelastic signal of topologically trivial dimerized chains is more pronounced within the bulk than at the edges.

Our main conclusion is that the topological degeneracy is generally more robust for chains with alternating AFM couplings, i.e., a spin variant of the SSH model, than for models mimicking Haldane chains, i.e., for alternating FM and AFM couplings. Higher robustness means here that, e.g., larger NNN couplings or stronger z-axis anisotropies can be added to the ideal chain without significantly coupling the edge states and thus destroying the topological phase.

We also discuss z-axis anisotropy for both alternating coupling constants because we wanted to discuss spin chains on surfaces and the direction perpendicular to the surface is clearly special. This agrees with earlier studies based on chains with periodic boundary conditions [33,36,73] that reported a similarly clear difference in robustness between the Haldane limit and the dimer regime for a slightly different variant of z-axis anisotropy.

While there are significant finite-size effects when AFM NNN couplings are involved, even relatively short chains support parameter regimes with reasonably protected edge-state degeneracy. Finite-size effects for FM NNN couplings are small; see Fig. 13. For z-axis anisotropy, our criterion of approximate ground-state degeneracy agrees reasonably well with phase diagrams based on more sophisticated approaches applicable to the TL [34,34,103,104]; see Figs. 14 and 15. This suggests that even rather short chains, which can be achieved in experiment, support observable signatures of topological edge-state degeneracy.

In agreement with results for SSH models with hard-core bosons [55] and in contrast to noninteracting bosons [53], we find that topological degeneracy can survive substantial NNN coupling. This can be related to the fact that our spin model with alternating stronger and weaker AFM bonds corresponds to a hard-core bosonic SSH model with additional inter-site density-density interactions. While this SSH-like scenario is more robust w.r.t. FM NNN coupling, AFM NNN couplings are the one aspect where the Haldane-like scenario offers more protection. Once z-axis anisotropy and NNN couplings are both active, dimerized SSH-like chains are again more robust than Haldane chains.

Edge states of topologically nontrivial spin systems have become an area of intense research, especially in two dimensions, e.g., for the Kitaev model [105–107]. In contrast to edge states of superconducting Kitaev chains, which can be observed in an STM [108], they are not charged, which makes them more challenging to investigate. This comes in addition to the fact that there is currently no clear route to the implementation of a Kitaev spin liquid on a surface. A new idea in this direction is the recent proposal to realize the Kitaev honeycomb model with quantum dots [109].

Our one-dimensional model is based on available building blocks, as the examination and manipulation of adatoms with an STM is a widely used method [13,80–87,94,95,110–114], and the reviews in Refs. [80,111,112] provide an overview of this topic. Such finite and imperfect spin chains may thus provide a feasible starting point for the observation of topologically protected edge states in microscopically assembled spin structures. This has been already exploited to measure edge states of the Haldane chain [46], where the splitting can

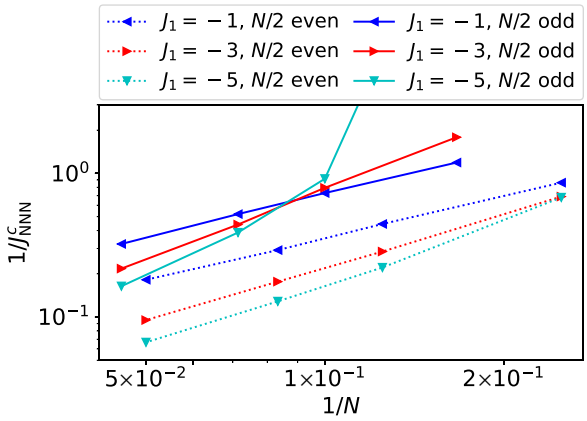

FIG. 17. Finite-size effect of the transition where $\Theta_{\mathrm{PT}} = 0.5$ in the upper left part of Fig. 13.

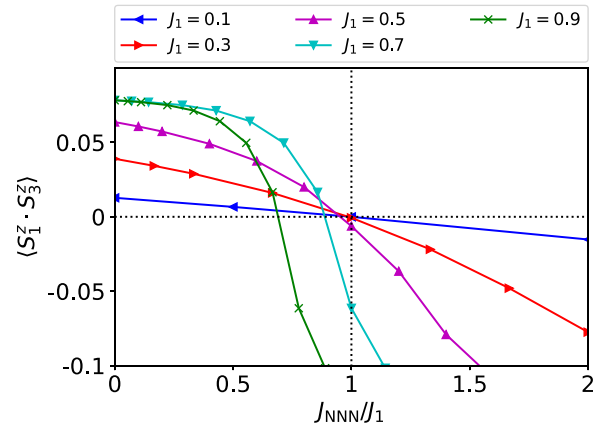

FIG. 18. Correlation function as a delimiter between the edge-state and the decoupled-chain origin of ground-state degeneracy in the upper right part of Fig. 13.

be reduced by making the chain longer. Splitting in the dimer scenario can be tuned by the ratio J_1/J_2, so that tunneling times can potentially be made shorter or longer by placing the dimers closer together or farther apart. Indeed, measurements of edge states in alternating spin-1/2 chains have been reported very recently [48,49].

ACKNOWLEDGMENT

The authors acknowledge support by the state of Baden-Württemberg through bwHPC.

APPENDIX: NNN-COUPLING

Figure 13 in the main text depicts the impact of NNN coupling on isotropic alternating chains. Here we add further insights to this figure.

Figure 17 illustrates the finite-size effects from the upper left part of Fig. 13. It shows the value J^c_{NNN}, where Θ_{PT} crosses $\Theta^{\mathrm{tran}}_{\mathrm{PT}} = 0.5$. Since $1/J^c_{\mathrm{NNN}}$ decreases as $1/N$ decreases, the transition in the upper left part of Fig. 13 diverges in the thermodynamic limit.

In the upper right part of Fig. 13, for an odd number $N/2$, there is a transition from a topologically fourfold degenerate ground state characterized by edge states to a fourfold degeneracy of decoupled chains, each with a ground-state doublet. Figure 18 illustrates that this transition can be identified by a change in the sign of the correlation function $\langle S^z_1 \cdot S^z_3 \rangle$. For strong dimerization $J_1 \ll 1$, this sign change occurs at $J_1 = J_{\mathrm{NNN}}$. This behavior can be attributed to frustration: when $J_1 > J_{\mathrm{NNN}}$, the AFM coupling J_1 is satisfied while J_{NNN} is not, resulting in $\langle S^z_1 \cdot S^z_3 \rangle > 0$. Conversely, when $J_1 < J_{\mathrm{NNN}}$, J_{NNN} is satisfied and $\langle S^z_1 \cdot S^z_3 \rangle < 0$. As J_1 approaches J_2, indicating weak dimerization, the weaker dimerization becomes the dominant contribution, shifting the transition point away from $J_1 = J_{\mathrm{NNN}}$.

[1] F. D. M. Haldane, Nobel lecture: Topological quantum matter, Rev. Mod. Phys. **89**, 040502 (2017).

[2] X.-G. Wen, *Colloquium*: Zoo of quantum-topological phases of matter, Rev. Mod. Phys. **89**, 041004 (2017).

[3] C.-K. Chiu, J. C. Y. Teo, A. P. Schnyder, and S. Ryu, Classification of topological quantum matter with symmetries, Rev. Mod. Phys. **88**, 035005 (2016).

[4] X.-L. Qi and S.-C. Zhang, Topological insulators and superconductors, Rev. Mod. Phys. **83**, 1057 (2011).

[5] M. Z. Hasan and C. L. Kane, *Colloquium*: Topological insulators, Rev. Mod. Phys. **82**, 3045 (2010).

[6] S. A. Wolf, D. D. Awschalom, R. A. Buhrman, J. M. Daughton, S. von Molnár, M. L. Roukes, A. Y. Chtchelkanova, and D. M. Treger, Spintronics: A spin-based electronics vision for the future, Science **294**, 1488 (2001).

[7] A. Hirohata, K. Yamada, Y. Nakatani, I.-L. Prejbeanu, B. Diény, P. Pirro, and B. Hillebrands, Review on spintronics: Principles and device applications, J. Magn. Magn. Mater. **509**, 166711 (2020).

[8] I. Žutić, J. Fabian, and S. Das Sarma, Spintronics: Fundamentals and applications, Rev. Mod. Phys. **76**, 323 (2004).

[9] S. D. Bader and S. S. P. Parkin, Spintronics, Annu. Rev. Condens. Matter Phys. **1**, 71 (2010).

[10] C. Dlaska, B. Vermersch, and P. Zoller, Robust quantum state transfer via topologically protected edge channels in dipolar arrays, Quantum Sci. Technol. **2**, 015001 (2017).

[11] N. Lang and H. P. Büchler, Topological networks for quantum communication between distant qubits, npj Quantum Inf. **3**, 47 (2017).

[12] C. Nayak, S. H. Simon, A. Stern, M. Freedman, and S. Das Sarma, Non-Abelian anyons and topological quantum computation, Rev. Mod. Phys. **80**, 1083 (2008).

[13] F. Delgado and J. Fernández-Rossier, Spin decoherence of magnetic atoms on surfaces, Prog. Surf. Sci. **92**, 40 (2017).

[14] A. Miyake, Quantum computation on the edge of a symmetry-protected topological order, Phys. Rev. Lett. **105**, 040501 (2010).

[15] I. Affleck, Quantum spin chains and the Haldane gap, J. Phys.: Condens. Matter **1**, 3047 (1989).

[16] J.-P. Renard, L.-P. Regnault, and M. Verdaguer, Haldane quantum spin chains, *Magnetism: Molecules to Materials I* (John Wiley & Sons, New York, NY, 2001), Chap. 2, pp. 49–93.

[17] F. Pollmann, E. Berg, A. M. Turner, and M. Oshikawa, Symmetry protection of topological phases in one-dimensional quantum spin systems, Phys. Rev. B **85**, 075125 (2012).

[18] F. D. M. Haldane, Continuum dynamics of the 1-D Heisenberg antiferromagnet: Identification with the $O(3)$ nonlinear sigma model, Phys. Lett. A **93**, 464 (1983).

[19] F. D. M. Haldane, Nonlinear field theory of large-spin Heisenberg antiferromagnets: Semiclassically quantized solitons of the one-dimensional easy-axis Néel state, Phys. Rev. Lett. **50**, 1153 (1983).

[20] G. Xu, J. F. DiTusa, T. Ito, K. Oka, H. Takagi, C. Broholm, and G. Aeppli, Y_2BaNiO_5: A nearly ideal realization of the $S = 1$ Heisenberg chain with antiferromagnetic interactions, Phys. Rev. B **54**, R6827 (1996).

[21] H. Mutka, J. L. Soubeyroux, G. Bourleaux, and P. Colombet, Support for the Haldane conjecture: Gap for magnetic excitations in the quasi-one-dimensional $S = 1$ Heisenberg antiferromagnet $AgVP_2S_6$, Phys. Rev. B **39**, 4820 (1989).

[22] J. P. Renard, M. Verdaguer, L. P. Regnault, W. A. C. Erkelens, J. Rossat-Mignod, J. Ribas, W. G. Stirling, and C. Vettier, Quantum energy gap in two quasi-one-dimensional $S = 1$ Heisenberg antiferromagnets (invited), J. Appl. Phys. **63**, 3538 (1988).

[23] W. J. L. Buyers, R. M. Morra, R. L. Armstrong, M. J. Hogan, P. Gerlach, and K. Hirakawa, Experimental evidence for the Haldane gap in a spin-1 nearly isotropic, antiferromagnetic chain, Phys. Rev. Lett. **56**, 371 (1986).

[24] J. P. Renard, M. Verdaguer, L. P. Regnault, W. A. C. Erkelens, J. Rossat-Mignod, and W. G. Stirling, Presumption for a quantum energy gap in the quasi-one-dimensional $S = 1$ Heisenberg antiferromagnet $Ni(C_2H_8N_2)_2NO_2(ClO_4)$, Europhys. Lett. **3**, 945 (1987).

[25] K. Katsumata, H. Hori, T. Takeuchi, M. Date, A. Yamagishi, and J. P. Renard, Magnetization process of an $S = 1$ linear-chain Heisenberg antiferromagnet, Phys. Rev. Lett. **63**, 86 (1989).

[26] R. M. Morra, W. J. L. Buyers, R. L. Armstrong, and K. Hirakawa, Spin dynamics and the Haldane gap in the spin-1 quasi-one-dimensional antiferromagnet $CsNiCl_3$, Phys. Rev. B **38**, 543 (1988).

[27] L. P. Regnault and J. P. Renard, Spin dynamics in the Haldane-gap system NENP, Phys. B: Condens. Matter **215**, 71 (1995).

[28] J. Darriet and L. P. Regnault, The compound Y_2BaNiO_5: A new example of a Haldane gap in a $S = 1$ magnetic chain, Solid State Commun. **86**, 409 (1993).

[29] Y. Ajiro, T. Goto, H. Kikuchi, T. Sakakibara, and T. Inami, High-field magnetization of a quasi-one-dimensional $S = 1$ antiferromagnet $Ni(C_2H_8N_2)_2NO_2(ClO_4)$: Observation of the Haldane gap, Phys. Rev. Lett. **63**, 1424 (1989).

[30] E. Čižmár, M. Ozerov, O. Ignatchik, T. P. Papageorgiou, J. Wosnitza, S. A. Zvyagin, J. Krzystek, Z. Zhou, C. P. Landee, B. R. Landry, M. M. Turnbull, and J. L. Wikaira, Magnetic properties of the Haldane-gap material $[Ni(C_2H_8N_2)_2NO_2](BF_4)$, New J. Phys. **10**, 033008 (2008).

[31] M. Kenzelmann, G. Xu, I. A. Zaliznyak, C. Broholm, J. F. DiTusa, G. Aeppli, T. Ito, K. Oka, and H. Takagi, Structure of end states for a Haldane spin chain, Phys. Rev. Lett. **90**, 087202 (2003).

[32] I. Affleck, T. Kennedy, E. H. Lieb, and H. Tasaki, Rigorous results on valence-bond ground states in antiferromagnets, Phys. Rev. Lett. **59**, 799 (1987).

[33] M. Yamanaka, Y. Hatsugai, and M. Kohmoto, Phase diagram of the $S = 1/2$ quantum spin chain with bond alternation, Phys. Rev. B **48**, 9555 (1993).

[34] K. Hida, Ground-state phase diagram of the spin-1/2 ferromagnetic-antiferromagnetic alternating Heisenberg chain with anisotropy, Phys. Rev. B **46**, 8268 (1992).

[35] K. Hida, Crossover between the Haldane-gap phase and the dimer phase in the spin-1/2 alternating Heisenberg chain, Phys. Rev. B **45**, 2207 (1992).

[36] M. Kohmoto and H. Tasaki, Hidden $Z_2 \times Z_2$ symmetry breaking and the Haldane phase in the $S = 1/2$ quantum spin chain with bond alternation, Phys. Rev. B **46**, 3486 (1992).

[37] M. Hagiwara, K. Katsumata, I. Affleck, B. I. Halperin, and J. P. Renard, Observation of $S = 1/2$ degrees of freedom in an $S = 1$ linear-chain Heisenberg antiferromagnet, Phys. Rev. Lett. **65**, 3181 (1990).

[38] S. Sahoo, D. Dey, S. K. Saha, and M. Kumar, Haldane and dimer phases in a frustrated spin chain: An exact ground state and associated topological phase transition, J. Phys.: Condens. Matter **32**, 335601 (2020).

[39] K. Hida and S. Takada, String order parameters in the Haldane gap phase of the spin-1/2 alternating Heisenberg chain—Numerical diagonalization and variational study–, J. Phys. Soc. Jpn. **61**, 1879 (1992).

[40] S. R. White, Equivalence of the antiferromagnetic Heisenberg ladder to a single $S = 1$ chain, Phys. Rev. B **53**, 52 (1996).

[41] S. H. Glarum, S. Geschwind, K. M. Lee, M. L. Kaplan, and J. Michel, Observation of fractional spin $S = 1/2$ on open ends of $S = 1$ linear antiferromagnetic chains: Nonmagnetic doping, Phys. Rev. Lett. **67**, 1614 (1991).

[42] S. Kimura, H. Ohta, M. Motokawa, T. Yokoo, and J. Akimitsu, $S = 1/2$ degrees of freedom in Haldane system Y_2BaNiO_5 observed by submillimeter wave ESR, J. Phys. Soc. Jpn. **67**, 2514 (1998).

[43] M. Yoshida, K. Shiraki, S. Okubo, H. Ohta, T. Ito, H. Takagi, M. Kaburagi, and Y. Ajiro, Energy structure of a finite Haldane chain in $Y_2BaNi_{0.96}Mg_{0.04}O_5$ studied by high field electron spin resonance, Phys. Rev. Lett. **95**, 117202 (2005).

[44] F. Tedoldi, R. Santachiara, and M. Horvatić, ^{89}Y NMR imaging of the staggered magnetization in the doped Haldane chain $Y_2BaNi_{1-x}Mg_xO5$, Phys. Rev. Lett. **83**, 412 (1999).

[45] F. Delgado, C. D. Batista, and J. Fernández-Rossier, Local probe of fractional edge states of $S = 1$ Heisenberg spin chains, Phys. Rev. Lett. **111**, 167201 (2013).

[46] S. Mishra, G. Catarina, F. Wu, R. Ortiz, D. Jacob, K. Eimre, J. Ma, C. A. Pignedoli, X. Feng, P. Ruffieux, J. Fernández-Rossier, and R. Fasel, Observation of fractional edge excitations in nanographene spin chains, Nature (London) **598**, 287 (2021).

[47] Y. Zhao, K. Jiang, C. Li, Y. Liu, G. Zhu, M. Pizzochero, E. Kaxiras, D. Guan, Y. Li, H. Zheng, C. Liu, J. Jia, M. Qin, X. Zhuang, and S. Wang, Quantum nanomagnets in on-surface metal-free porphyrin chains, Nat. Chem. **15**, 53 (2023).

[48] H. Wang, P. Fan, J. Chen, L. Jiang, H.-J. Gao, J. L. Lado, and K. Yang, Realizing topological quantum magnets with atomic spins on surfaces, arXiv:2403.14145.

[49] C. Zhao, G. Catarina, J.-J. Zhang, J. C. G. Henriques, L. Yang, J. Ma, X. Feng, O. Gröning, P. Ruffieux, J. Fernández-Rossier, and R. Fasel, Tunable topological phases in nanographene-based spin-1/2 alternating-exchange Heisenberg chains, arXiv:2402.13590.

[50] N. Chepiga and F. Mila, Exact zero modes in frustrated Haldane chains, Phys. Rev. B **96**, 060409(R) (2017).

[51] N. Chepiga and F. Mila, Rigorous decoupling between edge states in frustrated spin chains and ladders, Phys. Rev. B **97**, 174434 (2018).

[52] W. P. Su, J. R. Schrieffer, and A. J. Heeger, Solitons in polyacetylene, Phys. Rev. Lett. **42**, 1698 (1979).

[53] F. Grusdt, M. Höning, and M. Fleischhauer, Topological edge states in the one-dimensional superlattice Bose-Hubbard model, Phys. Rev. Lett. **110**, 260405 (2013).

[54] P. Jordan and E. Wigner, Ìber das paulische äquivalenzverbot, Z. Angew. Phys. **47**, 631 (1928).

[55] S. de Léséleuc, V. Lienhard, P. Scholl, D. Barredo, S. Weber, N. Lang, H. P. Büchler, T. Lahaye, and A. Browaeys, Observation of a symmetry-protected topological phase of interacting bosons with Rydberg atoms, Science **365**, 775 (2019).

[56] M. Chatterjee, M. Kumar, and Z. G. Soos, Spin-$\frac{1}{2}$ string correlations and singlet-triplet gaps of frustrated ladders with ferromagnetic legs and alternate ferromagnetic and antiferromagnetic rungs, Phys. Rev. B **109**, 094439 (2024).

[57] T. Barnes, J. Riera, and D. A. Tennant, $S = \frac{1}{2}$ alternating chain using multiprecision methods, Phys. Rev. B **59**, 11384 (1999).

[58] K. Hida, XY Phase in the ground state of the spin-1/2 anisotropic alternating Heisenberg chain, J. Phys. Soc. Jpn. **62**, 3357 (1993).

[59] M. S. Bahovadinov, O. Gülseren, and J. Schnack, Local entanglement and string order parameter in dimerized models, J. Phys.: Condens. Matter **31**, 505602 (2019).

[60] S. Sahoo, V. M. L. Durga Prasad Goli, D. Sen, and S. Ramasesha, Studies on a frustrated Heisenberg spin chain with alternating ferromagnetic and antiferromagnetic exchanges, J. Phys.: Condens. Matter **26**, 276002 (2014).

[61] S. Yoshida and K. Okamoto, Phase diagram of spin-1/2 alternating ferromagnetic chain with XY-like anisotropy, J. Phys. Soc. Jpn. **58**, 4367 (1989).

[62] R. Haghshenas, A. Langari, and A. T. Rezakhani, Symmetry fractionalization: Symmetry-protected topological phases of the bond-alternating spin-1/2 Heisenberg chain, J. Phys.: Condens. Matter **26**, 456001 (2014).

[63] K. Hida, Topological phases of spin-1/2 ferromagnetic-antiferromagnetic alternating Heisenberg chains with alternating next-nearest-neighbour interaction, J. Phys. Soc. Jpn. **85**, 124712 (2016).

[64] K. Hida, Characterization of topological phases of spin-1/2 frustrated ferromagnetic-antiferromagnetic alternating Heisenberg chains by entanglement spectrum, J. Phys. Soc. Jpn. **85**, 024705 (2016).

[65] G.-H. Liu, W.-L. You, W. Li, and G. Su, Quantum phase transitions and string orders in the spin-1/2 Heisenberg-Ising alternating chain with Dzyaloshinskii-Moriya interaction, J. Phys.: Condens. Matter **27**, 165602 (2015).

[66] H. T. Wang, B. Li, and S. Y. Cho, Topological quantum phase transition in bond-alternating spin-1/2 Heisenberg chains, Phys. Rev. B **87**, 054402 (2013).

[67] K. Hida, K. Takano, and H. Suzuki, Topological phases of the spin-1/2 ferromagnetic-antiferromagnetic alternating Heisenberg chain with frustrated next-nearest-neighbour interaction, J. Phys. Soc. Jpn. **82**, 064703 (2013).

[68] W. Duffy and K. P. Barr, Theory of alternating antiferromagnetic Heisenberg linear chains, Phys. Rev. **165**, 647 (1968).

[69] H. Manaka, I. Yamada, M. Hagiwara, and M. Tokunaga, High-field and high-frequency ESR study of the Haldane state formed in the ferromagnetic and antiferromagnetic alternating Heisenberg chain system $(CH_3)_2CHNH_3CuCl_3$, Phys. Rev. B **63**, 144428 (2001).

[70] M. Chatterjee, M. Kumar, and Z. G. Soos, Singlet quantum phases of the frustrated spin-1/2 ladder with ferromagnetic (F) exchange in legs and alternating F-AF exchange in rungs, Phys. Scr. **99**, 025973 (2024).

[71] A. Collins, C. J. Hamer, and Z. Weihong, Modified triplet-wave expansion method applied to the alternating Heisenberg chain, Phys. Rev. B **74**, 144414 (2006).

[72] M. Nakamura and S. Todo, Order parameter to characterize valence-bond-solid states in quantum spin chains, Phys. Rev. Lett. **89**, 077204 (2002).

[73] K. Hida, Ground-state phase diagram of the spin 1/2 alternating Heisenberg chain with anisotropy on the antiferromagnetic bond, J. Phys. Soc. Jpn. **62**, 1463 (1993).

[74] W.-X. Chen, J. Ren, W.-L. You, X. Hao, and Y.-Z. Wu, Phase diagram of the spin-1/2 Heisenberg alternating chain in a magnetic field, Commun. Theor. Phys. **71**, 1029 (2019).

[75] I. Maruyama, S. Tanaya, M. Arikawa, and Y. Hatsugai, Topological identification of location of spin–singlet pairs and edge states, J. Phys.: Conf. Ser. **200**, 022075 (2010).

[76] Alternatively, mapping isotropic Heisenberg exchange onto bosons generates intersite density-density interactions in addition to the onsite hard-core constraint.

[77] T. Kennedy, Exact diagonalisations of open spin-1 chains, J. Phys.: Condens. Matter **2**, 5737 (1990).

[78] S. Yamamoto and S. Miyashita, Anisotropy effects on the magnetic properties of an $S = 1$ antiferromagnetic Heisenberg chain, Phys. Rev. B **50**, 6277 (1994).

[79] S. Miyashita and S. Yamamoto, Effects of edges in $S = 1$ Heisenberg antiferromagnetic chains, Phys. Rev. B **48**, 913 (1993).

[80] J.-P. Gauyacq, N. Lorente, and F. D. Novaes, Excitation of local magnetic moments by tunneling electrons, Prog. Surf. Sci. **87**, 63 (2012).

[81] C. F. Hirjibehedin, C. P. Lutz, and A. J. Heinrich, Spin coupling in engineered atomic structures, Science **312**, 1021 (2006).

[82] P. Gambardella, S. Rusponi, M. Veronese, S. S. Dhesi, C. Grazioli, A. Dallmeyer, I. Cabria, R. Zeller, P. H. Dederichs, K. Kern, C. Carbone, and H. Brune, Giant magnetic anisotropy of single cobalt atoms and nanoparticles, Science **300**, 1130 (2003).

[83] S. Loth, S. Baumann, C. P. Lutz, D. M. Eigler, and A. J. Heinrich, Bistability in atomic-scale antiferromagnets, Science **335**, 196 (2012).

[84] C. F. Hirjibehedin, C.-Y. Lin, A. F. Otte, M. Ternes, C. P. Lutz, B. A. Jones, and A. J. Heinrich, Large magnetic anisotropy of

a single atomic spin embedded in a surface molecular network, Science **317**, 1199 (2007).
[85] B. Bryant, A. Spinelli, J. J. T. Wagenaar, M. Gerrits, and A. F. Otte, Local control of single atom magnetocrystalline anisotropy, Phys. Rev. Lett. **111**, 127203 (2013).
[86] J. Fernández-Rossier, Theory of single-spin inelastic tunneling spectroscopy, Phys. Rev. Lett. **102**, 256802 (2009).
[87] D.-J. Choi, R. Robles, S. Yan, J. A. J. Burgess, S. Rolf-Pissarczyk, J.-P. Gauyacq, N. Lorente, M. Ternes, and S. Loth, Building complex Kondo impurities by manipulating entangled spin chains, Nano Lett. **17**, 6203 (2017).
[88] Y.-C. Tzeng, H. Onishi, T. Okubo, and Y.-J. Kao, Quantum phase transitions driven by rhombic-type single-ion anisotropy in the $S = 1$ Haldane chain, Phys. Rev. B **96**, 060404(R) (2017).
[89] S. C. Furuya, T. Suzuki, S. Takayoshi, Y. Maeda, and M. Oshikawa, Single-ion anisotropy in Haldane chains and the form factor of the $O(3)$ nonlinear sigma model, Phys. Rev. B **84**, 180410(R) (2011).
[90] O. Golinelli, T. Jolicoeur, and R. Lacaze, Haldane gaps in a spin-1 Heisenberg chain with easy-plane single-ion anisotropy, Phys. Rev. B **45**, 9798 (1992).
[91] Y. Hatsugai and M. Kohmoto, Numerical study of the hidden antiferromagnetic order in the Haldane phase, Phys. Rev. B **44**, 11789 (1991).
[92] M. den Nijs and K. Rommelse, Preroughening transitions in crystal surfaces and valence-bond phases in quantum spin chains, Phys. Rev. B **40**, 4709 (1989).
[93] H. Tasaki, Quantum liquid in antiferromagnetic chains: A stochastic geometric approach to the Haldane gap, Phys. Rev. Lett. **66**, 798 (1991).
[94] M. Moro-Lagares, R. Korytár, M. Piantek, R. Robles, N. Lorente, J. I. Pascual, M. R. Ibarra, and D. Serrate, Real space manifestations of coherent screening in atomic scale Kondo lattices, Nat. Commun. **10**, 2211 (2019).
[95] R. Toskovic, R. van den Berg, A. Spinelli, I. S. Eliens, B. van den Toorn, B. Bryant, J.-S. Caux, and A. F. Otte, Atomic spin-chain realization of a model for quantum criticality, Nat. Phys. **12**, 656 (2016).
[96] A. Machens, N. P. Konstantinidis, O. Waldmann, I. Schneider, and S. Eggert, Even-odd effect in short antiferromagnetic Heisenberg chains, Phys. Rev. B **87**, 144409 (2013).
[97] A. Ruhe, Implementation aspects of band Lanczos algorithms for computation of eigenvalues of large sparse symmetric matrices, Math. Comput. **33**, 680 (1979).
[98] D. Dey, M. Kumar, and Z. G. Soos, Boundary-induced spin-density waves in linear Heisenberg antiferromagnetic spin chains with $S \geqslant 1$, Phys. Rev. B **94**, 144417 (2016).
[99] H. Watanabe, Numerical diagonalization study of an $S = 1/2$ ladder model with open boundary conditions, Phys. Rev. B **50**, 13442 (1994).
[100] E. Lieb and D. Mattis, Ordering energy levels of interacting spin systems, J. Math. Phys. **3**, 749 (1962).
[101] E. R. Gagliano and C. A. Balseiro, Dynamical properties of quantum many-body systems at zero temperature, Phys. Rev. Lett. **59**, 2999 (1987).
[102] E. R. Gagliano and C. A. Balseiro, Dynamic correlation functions in quantum many-body systems at zero temperature, Phys. Rev. B **38**, 11766 (1988).
[103] M. Yamanaka, Y. Hatsugai, and M. Kohmoto, Phase diagram of the Ashkin-Teller quantum spin chain, Phys. Rev. B **50**, 559 (1994).
[104] K.-i. Funase and S. Yamamoto, Effects of edges in spin-1/2 bond-alternating Heisenberg chains: Matrix-product variational approach, Phys. Lett. A **334**, 220 (2005).
[105] J. Feldmeier, W. Natori, M. Knap, and J. Knolle, Local probes for charge-neutral edge states in two-dimensional quantum magnets, Phys. Rev. B **102**, 134423 (2020).
[106] M. Udagawa, S. Takayoshi, and T. Oka, Scanning tunneling microscopy as a single Majorana detector of Kitaev's chiral spin liquid, Phys. Rev. Lett. **126**, 127201 (2021).
[107] E. J. König, M. T. Randeria, and B. Jäck, Tunneling spectroscopy of quantum spin liquids, Phys. Rev. Lett. **125**, 267206 (2020).
[108] B. Jäck, Y. Xie, and A. Yazdani, Detecting and distinguishing Majorana zero modes with the scanning tunnelling microscope, Nat. Rev. Phys. **3**, 541 (2021).
[109] T. Cookmeyer and S. Das Sarma, Phys. Rev. Lett. **132**, 186501 (2024).
[110] A. A. Khajetoorians, J. Wiebe, B. Chilian, S. Lounis, S. Blügel, and R. Wiesendanger, Atom-by-atom engineering and magnetometry of tailored nanomagnets, Nat. Phys. **8**, 497 (2012).
[111] D.-J. Choi, N. Lorente, J. Wiebe, K. von Bergmann, A. F. Otte, and A. J. Heinrich, *Colloquium*: Atomic spin chains on surfaces, Rev. Mod. Phys. **91**, 041001 (2019).
[112] R. Wiesendanger, Spin mapping at the nanoscale and atomic scale, Rev. Mod. Phys. **81**, 1495 (2009).
[113] D. Serrate, P. Ferriani, Y. Yoshida, S.-W. Hla, M. Menzel, K. von Bergmann, S. Heinze, A. Kubetzka, and R. Wiesendanger, Imaging and manipulating the spin direction of individual atoms, Nat. Nanotechnol. **5**, 350 (2010).
[114] A. A. Khajetoorians, J. Wiebe, B. Chilian, and R. Wiesendanger, Realizing all-spin–based logic operations atom by atom, Science **332**, 1062 (2011).